
Pergamon

J. Mech. Phys. Solids, Vol. 46, No. 12, pp. 2361–2386, 1998

Printed in Great Britain
0022–5096/98 $—see front matter

PII: S0022–5096(98)00061–1

LIMITATIONS TO LEADING-ORDER ASYMPTOTIC SOLUTIONS FOR ELASTIC–PLASTIC CRACK GROWTH

W. J. DRUGAN

Department of Engineering Physics, University of Wisconsin-Madison, 1500 Engineering Drive, Madison, WI 53706, U.S.A.

(*Received* 18 *November* 1997)

ABSTRACT

Previous work has shown that there are significant discrepancies between leading-order asymptotic analytical solutions for the elastic–plastic fields near growing crack tips and detailed numerical finite element solutions of the same problems. The evidence is clearest in the simplest physically realistic case: quasi-static anti-plane shear crack growth in homogeneous, isotropic elastic–ideally plastic material. There, the sole extant asymptotic analytical solution involves a plastic loading sector of radial stress characteristics extending about 20° from ahead of the crack, followed by elastic unloading, whereas detailed numerical finite element solutions show the presence of an additional sector of plastic loading, extending from about 20 to about 50°, that is comprised of non-radial characteristics. To explore how the asymptotic analysis can completely miss this important solution feature, we derive an exact representation for the stress and deformation fields in such a propagating region of non-radial characteristics, as well as in the other allowable solution regions. These exact solutions contain arbitrary functions, which are determined by applying asymptotic analysis to the *solutions* and assembling a complete near-tip solution, valid through second order, that is in agreement with the numerical finite element results. In so doing, we prove that the angular extent of the sector of non-radial characteristics, while substantial until extremely close to the crack tip, vanishes in the limit as the tip is approached, and that the solution in this sector is not of variable–separable form. Beyond resolving the analytical–numerical discrepancies in this specific anti-plane shear problem, the analysis serves to caution, by explicit example, that purely leading-order asymptotic solutions to nonlinear crack growth problems cannot in general capture all essential physical features of the near-tip fields, and that the often-invoked assumption of variable–separable solutions is not always valid.

Keywords: A. crack propagation, A. crack tip plasticity, B. crack mechanics, B. elastic–plastic material, C. asymptotic analysis.

1. INTRODUCTION

It is by now well-known and experimentally documented that the ductile fracture process in many metals, metal–matrix composites and along ductile–brittle interfaces involves a stage in which a crack grows slowly and stably under increasing applied load until final instability occurs, and that this stage accounts for a substantial portion—often the majority—of a material's overall fracture toughness. Thus, analytical solutions for the fields produced by a growing crack in such materials have long been recognized as important to fundamental understanding of the ductile fracture process, and to quantitative prediction of final fracture. Due to the difficult nonlinear equations involved, no complete (i.e., full-field) analytical solutions have

been found for these growing crack elastic–plastic fields; rather, analytical progress has been limited to asymptotic solutions (valid for $r \to 0$, where r is distance from the crack tip). Key issues relating to such solutions are their completeness (that is, their ability to characterize the near-tip state for any far-field geometry and loading) and their radius of validity; such obviously bear on the physical applicability of these solutions.

Perhaps the simplest physically realistic model of elastic–plastic crack growth is that of anti-plane shear (Mode III) quasi-static growth in a homogeneous, isotropic, elastic–ideally plastic flow-theory material. An asymptotic ($r \to 0$) solution for this case was first obtained by Chitaley and McClintock (1971); on either side of the antisymmetry plane, this solution involves a plastically deforming sector, comprised of a centered fan of characteristics, extending 19.7° from the crack plane, followed by a large elastic unloading sector, followed by a very small (0.37°) plastic reloading sector adjacent to the crack flank. No other asymptotic solutions for Mode III crack growth in such material have been found, yet the Chitaley–McClintock solution has the physically unsettling feature that the leading-order stress and velocity field amplitudes and distributions about the growing crack tip are completely specified by the asymptotic analysis.

Dean and Hutchinson (1980) performed a detailed full-field numerical finite element analysis of steady-state, small-scale yielding Mode III crack growth in the same material model, which they suggest should be accurate down to a radius from the crack tip of about 1% of the plastic zone size. Their near-tip elastic–plastic fields differ significantly from the asymptotic ones of Chitaley–McClintock: in particular, the numerical solution shows an additional plastically active region, of non-centered characteristics, directly following the centered fan region, extending from about 20 to about 41°. An independent numerical finite element analysis of the same problem, with significantly higher accuracy, was performed by Freund and Douglas (1982) as a special case of their dynamic elastic–plastic crack growth study. For the quasi-static growth case, they also found the additional plastically active region, of non-centered characteristics, directly following the centered fan region; their solution showed it to extend from about 20 to about 50°.

Thus, these numerical solutions show that there is an important conceptual feature of the elastic–plastic growing crack fields—a plastically deforming sector of non-centered characteristics subtending about 30° and extending as close to the crack tip as numerical resolution has allowed investigation—that is completely missed by the leading-order asymptotic solution of Chitaley and McClintock (1971). It seems important to resolve this discrepancy, both to fully understand the specific problem under discussion, but more generally to demonstrate explicitly what can happen when leading-order asymptotic analytical solutions are constructed for growing crack tip fields. This should have implications in the more complicated situations involving other loading modes, effects of inertia, more complex material behavior and effects of heterogeneity.

The anti-plane shear problem has been chosen here because not only is it the simplest conceptually, and thus disconcerting to have such an apparent anomaly, but, as will be shown, one can make the greatest progress analytically. In contrast to previous analytical work on this problem, in which one first derives asymptotic

($r \to 0$) forms of the governing equations and then solves these, we shall show that an exact analytical solution can be derived for the stress and velocity fields everywhere in a plastically deforming region attending a steadily-growing crack, in terms of initially undetermined functions, and that one can derive such exact representations in the other permissible solution regions too. Asymptotics will then be applied to these *solutions* to show how a plastically deforming region of non-centered characteristics can follow the centered fan sector, how this permits reconciliation between the analytical and numerical solutions and how it affects the growing crack fields.

2. FORMULATION

We will employ a small-displacement-gradient formulation to analyze anti-plane shear (Mode III) quasi-static crack growth in homogeneous, isotropic elastic–ideally plastic material via an incremental (flow) theory. With respect to Fig. 1, Cartesian (x_1, x_2) and polar (r, θ) coordinate systems are both centered at the crack tip and move with it during crack growth, which is assumed to occur in the x_1-direction, with the straight crack front parallel to x_3. Angle θ is measured counterclockwise from the x_1-axis, and the crack growth speed is $\dot{a}$.

The governing equations are as follows. For the case of anti-plane shear crack growth, the velocity field has the form, in the coordinate system of Fig. 1

$$v_1 = v_2 \equiv 0; \quad v_3 = v_3(x_1, x_2). \tag{1}$$

Application of (1) to the general governing equations for the material class under consideration shows that the only nonzero components of stress and deformation-rate are the 13 (=31) and 23 (=32) components, and that these will at most be functions of (x_1, x_2). Thus, these governing equations reduce to the following, expressed for later convenience in terms of both the Cartesian and polar coordinate systems of Fig. 1:

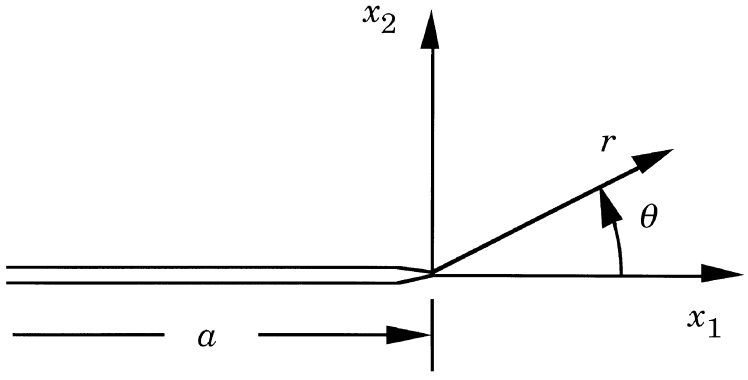

Fig. 1. Cartesian x_1, x_2 and polar r, θ coordinate systems are centered at the crack tip and move with it through the material during crack growth.

$$\frac{\partial \sigma_{13}}{\partial x_1} + \frac{\partial \sigma_{23}}{\partial x_2} = 0 \quad \text{or} \quad \frac{\partial \sigma_{r3}}{\partial r} + \frac{1}{r}\frac{\partial \sigma_{\theta 3}}{\partial \theta} + \frac{\sigma_{r3}}{r} = 0, \tag{2a,b}$$

$$\sigma_{13}^2 + \sigma_{23}^2 = k^2 \quad \text{or} \quad \sigma_{r3}^2 + \sigma_{\theta 3}^2 = k^2, \tag{3a,b}$$

$$D_{13} = \frac{1}{2}\frac{\partial v_3}{\partial x_1}, \quad D_{23} = \frac{1}{2}\frac{\partial v_3}{\partial x_2} \quad \text{or} \quad D_{r3} = \frac{1}{2}\frac{\partial v_3}{\partial r}, \quad D_{\theta 3} = \frac{1}{2r}\frac{\partial v_3}{\partial \theta}, \tag{4a,b}$$

$$D_{i3} = \frac{1}{2G}(\dot{\boldsymbol{\sigma}})_{i3} + \dot{\Lambda}\sigma_{i3}. \tag{5}$$

These represent the requirements of: equilibrium absent body forces (2); the Huber–Mises or Tresca yield condition, which are identical in anti-plane shear (3); compatibility in terms of rate-of-deformation tensor components (4); and the Prandtl–Reuss flow rule (5), in which subscript i has range 1,2 or r, θ. Here, k is the (constant) yield stress in pure shear; G is the elastic shear modulus; $\dot{\Lambda} \geqslant 0$ is a constitutively undetermined parameter; and a superposed dot denotes time rate at a fixed material point. Thus, in regions of ongoing plastic deformation, (3) and (5) must be satisfied with $\dot{\Lambda} > 0$; in material experiencing instantaneously elastic response, whether or not it has previously deformed plastically, (5) applies with $\dot{\Lambda} \equiv 0$ and (3) must be satisfied with $\leqslant$ replacing $=$. We shall assume that crack growth is steady-state with respect to an observer moving with the crack tip. Then, the material time rate of stress needed in (5) is obtained via the chain rule,

$$\dot{\boldsymbol{\sigma}} = -\dot{a}\frac{\partial \boldsymbol{\sigma}}{\partial x_1} = -\dot{a}\left(\cos\theta\frac{\partial \boldsymbol{\sigma}}{\partial r} - \frac{\sin\theta}{r}\frac{\partial \boldsymbol{\sigma}}{\partial \theta}\right). \tag{6}$$

It is well-known that in regions at yield, the stress state takes a particularly simple form when expressed in terms of stress characteristics: As illustrated in Fig. 2, it is always possible to rotate an element experiencing a stress state at yield to an orientation in which only one shearing component of stress acts, which via (3) must have magnitude k. Then, introduce an orthogonal curvilinear coordinate system (α, β) as illustrated, such that these directions are always normal and tangent, respectively, to

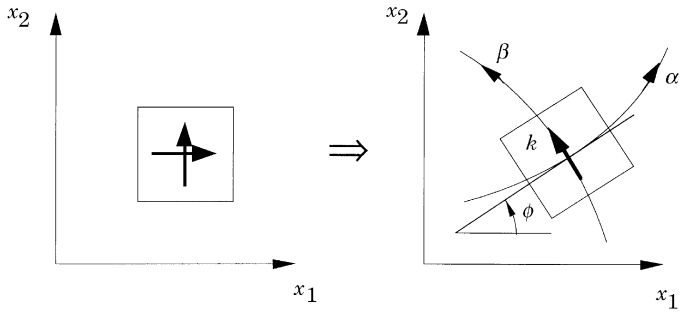

Fig. 2. Representation of the stress state at any point within a region at yield.

this shearing direction. Let ϕ measure the angle between the x_1-axis and the tangent to the α-line, so that

$$\frac{dx_2}{dx_1} = \tan\phi \quad \text{on } \alpha\text{-lines.} \tag{7}$$

In terms of the (α, β, x_3) coordinate system, the stress state at any point in a yielded region is thus,

$$\sigma_{\alpha 3} = 0, \quad \sigma_{\beta 3} = k, \tag{8}$$

so that by a simple stress transformation, the Cartesian components of stress are

$$\sigma_{13} = -k\sin\phi, \quad \sigma_{23} = k\cos\phi. \tag{9}$$

Substitution of (9) into equilibrium (2a) gives the requirement

$$-k\cos\phi\frac{\partial\phi}{\partial x_1} - k\sin\phi\frac{\partial\phi}{\partial x_2} = 0. \tag{10}$$

Also, since $\phi = \phi(x_1, x_2)$, the chain rule gives

$$d\phi = \frac{\partial\phi}{\partial x_1}dx_1 + \frac{\partial\phi}{\partial x_2}dx_2. \tag{11}$$

Combining (7), (10), (11), one finds the equilibrium requirement to reduce to

$$d\phi = 0 \quad \text{along } \alpha\text{-lines;} \tag{12}$$

that is, the α-lines, which are the stress characteristics, must always be straight. Thus, the stress state in any region at yield can be represented by a family of straight α-lines, on which the stress state is given by (8).

3. ASYMPTOTIC SOLUTIONS TO THE GOVERNING EQUATIONS

3.1. *Admissible types of near-tip solution sector*

Despite the relative simplicity of the anti-plane shear form of the governing equations compared, e.g., to plane strain, it nevertheless appears that closed-form analytical representations of the *growing* crack stress and deformation fields at all angles about the crack tip are only possible asymptotically, for $r \to 0$. Rice (1982) has given a general analysis and review of leading-order (in r) asymptotic solutions for elastic–plastic crack growth; here we briefly review these results for the Mode III problem. Stress boundedness demanded by (3) with some plausible existence assumptions on stress derivatives (Drugan, 1985) requires that

$$r\frac{\partial\sigma_{i3}}{\partial r} \to 0 \quad \text{as } r \to 0, \quad i = 1, 2, \quad \text{or} \quad r, \theta, \tag{13}$$

and thus the asymptotic ($r \to 0$) form of equilibrium (2b) is

$$\frac{\partial \sigma_{\theta 3}}{\partial \theta} + \sigma_{r3} = 0. \tag{14}$$

The asymptotic form of the flow rule is obtained by first applying (13) to (6) to find

$$r\dot{\boldsymbol{\sigma}} = \dot{a} \sin\theta \frac{\partial \boldsymbol{\sigma}}{\partial \theta} \quad \text{as } r \to 0, \tag{15}$$

so that (5) becomes, to leading order as $r \to 0$

$$D_{i3} = \frac{1}{2G}\frac{\dot{a}}{r} \sin\theta \left(\frac{\partial \boldsymbol{\sigma}}{\partial \theta}\right)_{i3} + \dot{\Lambda}\sigma_{i3}, \tag{16}$$

where again index i has range 1, 2 or r, θ, and we observe that, exactly,

$$\left(\frac{\partial \boldsymbol{\sigma}}{\partial \theta}\right)_{r3} = \frac{\partial \sigma_{r3}}{\partial \theta} - \sigma_{\theta 3}, \quad \left(\frac{\partial \boldsymbol{\sigma}}{\partial \theta}\right)_{\theta 3} = \frac{\partial \sigma_{\theta 3}}{\partial \theta} + \sigma_{r3}. \tag{17}$$

When (14) is applied to the θ-derivative of yield (3b), one finds that in near-tip ($r \to 0$) plastic regions

$$\sigma_{r3}\left(\frac{\partial \sigma_{r3}}{\partial \theta} - \sigma_{\theta 3}\right) = 0. \tag{18}$$

This implies that there are only two possible types of near-tip at-yield solution sector:

(i) *"Centered fan" plastic sectors*, in which $\sigma_{r3} = 0$, so that from (14) and (3b)

$$\sigma_{r3} = 0, \quad \sigma_{\theta 3} = \pm k; \tag{19}$$

(ii) *"Constant stress" plastic sectors*, in which $\partial \sigma_{r3}/\partial \theta - \sigma_{\theta 3} = 0$, so that from (14) and a stress transformation

$$\sigma_{13} = \text{constant}, \quad \sigma_{23} = \text{constant}, \tag{20}$$

where the constants satisfy (3a).

The third and final possible type of near-tip solution sector is one in which the rate of deformation is purely elastic, so that $\dot{\Lambda} \equiv 0$ in (16). In such a sector, the asymptotic stress field is governed by equilibrium (14) and the following compatibility requirement applied to (16) with $\dot{\Lambda} \equiv 0$:

$$\frac{\partial D_{r3}}{\partial \theta} - \frac{\partial (rD_{\theta 3})}{\partial r} = 0 \quad \Rightarrow \quad \frac{\partial}{\partial \theta}\left[\sin\theta \left(\frac{\partial \sigma_{r3}}{\partial \theta} - \sigma_{\theta 3}\right)\right] = 0. \tag{21}$$

Simultaneous solution of (14) and (21) gives the leading-order stress field for an instantaneously elastic sector:

$$\sigma_{23} = (A + B\theta)k, \quad \sigma_{13} = (C + B \ln|\sin\theta|)k, \tag{22}$$

where A, B and C are constants. Use of (22) in the $r3$ component of (16) with $\dot{\Lambda} \equiv 0$ gives, after integration by r and then enforcing the $\theta 3$ component of (16), the leading-order velocity field in such a sector (absent rigid-body motion):

$$v_3 = -B\frac{k}{G}\dot{a}\ln\left(\frac{R}{r}\right), \tag{23}$$

where R is an undetermined constant with length dimensions.

3.2. *Exact solution in the centered fan plastic sector*

Observe that the asymptotic stress field solution in the centered fan plastic sector, given in (19), corresponds to α-lines (stress characteristics) that are rays emanating from the crack tip. Now, as reviewed at the end of Section 2, stress characteristics must be straight lines everywhere in regions at yield. Thus, we immediately conclude that the exact representation for the stress field everywhere in a centered fan plastic sector (i.e., from the crack tip all the way to the elastic–plastic boundary) is that of (19), namely (choosing the + sign, as will apply in our solutions)

$$\boxed{\sigma_{r3} \equiv 0, \quad \sigma_{\theta 3} = +k}. \tag{24}$$

We now apply the full (i.e., not restricted to small r) form of the flow rule for steady-state crack growth, (5) with (6) and (17), together with the exact stress field (24), to calculate the exact velocity and $\dot{\Lambda}$ fields everywhere in a centered fan sector. The $r3$ component of (5) gives exactly:

$$D_{r3} = \frac{1}{2}\frac{\partial v_3}{\partial r} = \frac{1}{2G}\left[\frac{\dot{a}}{r}\sin\theta(-k)\right], \tag{25}$$

integration of which gives the exact velocity field representation

$$\boxed{v_3 = \dot{a}\frac{k}{G}\left[\sin\theta\ln\left(\frac{R}{r}\right)+f(\theta)\right]}, \tag{26}$$

where $f(\theta)$ is an undetermined function of integration. Then, using (26), the $\theta 3$ component of (5) can be solved for the exact $\dot{\Lambda}$ field:

$$\boxed{\dot{\Lambda} = \frac{\dot{a}}{2Gr}\left[\cos\theta\ln\left(\frac{R}{r}\right)+f'(\theta)\right]}. \tag{27}$$

Of course (24)–(27) are also valid asymptotically as $r \to 0$.

Rice (1968) showed for steady-state crack growth that (26) can be written as

$$v_3 = \dot{a}\frac{k}{G}\sin\theta\ln\left(\frac{eR_p(\theta)}{r}\right), \tag{28}$$

where e is the natural logarithm base and $R_p(\theta)$ is the location of the elastic–plastic boundary. For the special case of small-scale yielding crack growth, to be considered later, Freund and Douglas' (1982) numerical finite element results for the quasi-statically growing crack show that for all angles *within the centered fan region*, an excellent approximation is:

$$R_p(\theta) = 0.295\left(\frac{K}{k}\right)^2 \cos\theta, \tag{29}$$

where K is the Mode III stress intensity factor. Thus, for small-scale yielding steady-state crack growth, comparison of (26) with (28) and (29) shows we may write:

$$R = 0.802\left(\frac{K}{k}\right)^2, \quad f(\theta) = \sin\theta \ln(\cos\theta). \tag{30}$$

3.3. *Chitaley–McClintock asymptotic sector assembly*

Chitaley and McClintock (1971) provided the first complete near-tip solution to the stress and deformation fields near a growing Mode III crack in the material under consideration, by showing that the near-tip solution sectors just discussed can be assembled in the manner shown in Fig. 3 such that all boundary and continuity conditions are satisfied and so that $\dot{\Lambda} \geqslant 0$ everywhere. As the figure shows, the solution involves a centered fan plastic sector ahead of the crack, joined to an elastic unloading sector at $\theta \approx 19.71^\circ$, which extends to a very small constant stress plastic sector at $\theta \approx 179.63^\circ$.

The dominant terms for $r \to 0$ in the stress and velocity fields are summarized below:

$0 \leqslant \theta \leqslant 19.71^\circ$:

$$\sigma_{r3} = 0, \quad \sigma_{\theta 3} = +k, \quad v_3 = \frac{k}{G}\dot{a}\sin\theta \ln\left(\frac{R}{r}\right)$$

$19.71^\circ \leqslant \theta \leqslant 179.63^\circ$:

$$\sigma_{23} = (A + B\theta)k, \quad \sigma_{13} = (C + B\ln|\sin\theta|)k, \quad v_3 = -B\frac{k}{G}\dot{a}\ln\left(\frac{R}{r}\right)$$

$179.63^\circ \leqslant \theta \leqslant 180^\circ$:

$$\sigma_{13} = k, \quad \sigma_{23} = 0, \quad v_3 = -B\frac{k}{G}\dot{a}\ln\left(\frac{R}{r}\right), \tag{31}$$

where

$$A = 1.0574, \quad B = -0.33728, \quad C = -0.70385.$$

Observe from these that the Chitaley–McClintock solution completely specifies the

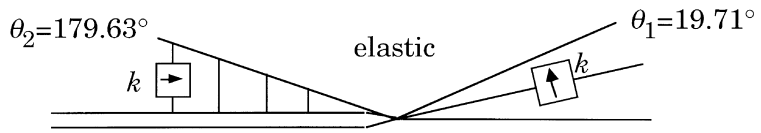

Fig. 3. The Chitaley–McClintock near-tip solution for a growing crack.

leading-order near-tip stress and deformation fields from the asymptotic analysis alone : everything is specified in the system (31) except the scaling parameter R. Thus, it is very difficult to see how this solution could describe the actual fields over a region of physically significant size near a Mode III growing crack, since one would anticipate that different far-field geometries and loadings would surely affect the crack fields in such a region, as they do e.g. for cracks in linear elastic materials. Further, the Chitaley–McClintock solution appears to be substantially different from the results of detailed numerical finite element simulations of Mode III crack growth, as noted earlier and discussed in further detail in the next section. Nevertheless, the asymptotic analysis approach just reviewed does not appear to permit any other leading-order solutions that satisfy all requisite conditions. A new analytical approach, directed at resolving this apparent discrepancy, is the subject of the remainder of the paper.

4. NEW ANALYTICAL APPROACH TO SOLUTION OF GROWING CRACK FIELDS

4.1. *Motivation*

We have just reviewed the fact that the Chitaley and McClintock (1971) solution for the leading-order stress and deformation fields is not capable of reflecting different far-field specimen geometries and loadings. Further evidence that the Chitaley–McClintock asymptotic solution does not in general represent the state of affairs over a physically significant radius at all angles about a growing crack tip is provided by the detailed numerical finite element steady-state crack growth solutions of Dean and Hutchinson (1980) and Freund and Douglas (1982). These authors carried out small-scale yielding solutions for Mode III quasi-static elastic–ideally plastic crack growth in the same material model employed here. The key results of the Dean–Hutchinson analysis are conveyed in Fig. 4, which is a reproduction of Fig. 3 of their paper. In this figure, the straight lines are stress characteristics, or α-lines, described above. The solution shows an active plastic region which, close to the crack tip, extends from the line ahead of the crack up to about $\theta \approx 41^\circ$, clearly greatly at variance with the 19.71° prediction of the Chitaley–McClintock solution. Since Dean and Hutchinson's near-tip quadrilateral elements were 0.4% of the maximum plastic zone radius, they concluded that assuming the Chitaley–McClintock asymptotic solution to be correct, it must be attained within a near-tip radius that is less than 1% of the plastic zone size. Furthermore, although these numerical results do appear to show that the stress characteristics in the range $0 \leqslant \theta < 20^\circ$ emanate from the crack tip, and hence appear to comprise a centered fan plastic region, those in the remaining plastic range appear *not* to emanate from the crack tip.

The Freund and Douglas (1982) solution confirms these conclusions, and implies an even smaller potential radius of validity for the asymptotic solution. Figure 5 shows the elastic–plastic boundary determined by the more accurate Freund–Douglas computation, for the stationary and quasi-statically growing crack cases; it is a reproduction of Fig. 5 of their paper with the dynamic results removed. As compared to the Dean–Hutchinson solution, the Freund–Douglas growing crack results exhibit

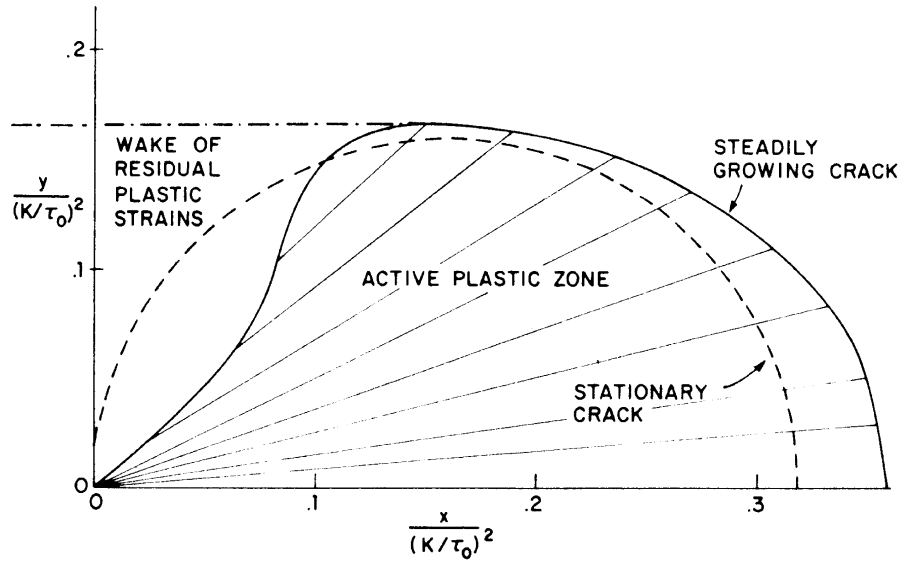

Fig. 4. The Dean and Hutchinson (1980) small-scale yielding steady-state crack growth solution.

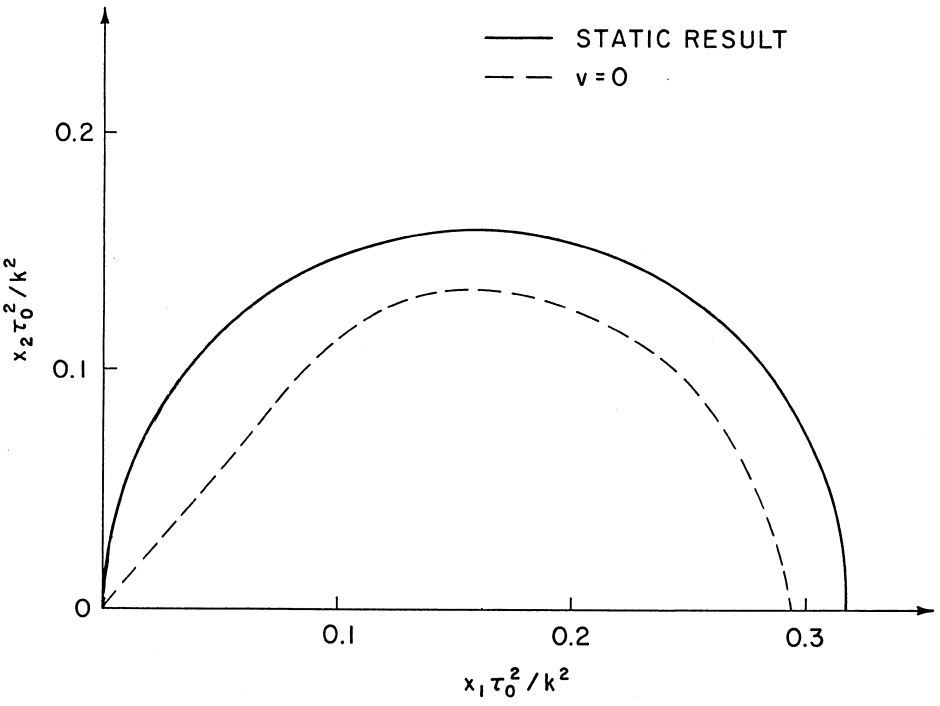

Fig. 5. The Freund and Douglas (1982) small-scale yielding steady-state crack growth solution ; the elastic–plastic boundary is represented by the dashed line (solid line—stationary crack).

a plastic zone that extends from the line ahead of the crack to about 50°, with the unloading boundary being nearly a straight radial line at this angle; also, the maximum radial extent of the plastic zone is about 20% less than that of Dean and Hutchinson. Although Freund and Douglas did not plot the stress characteristics, they commented that the principal shear direction did appear to be essentially radial only in the range $0 \leqslant \theta < 20^\circ$, thus confirming the Dean–Hutchinson findings while exhibiting an even larger angular range of nonradial stress characteristics (roughly $20^\circ < \theta < 50^\circ$).

These solutions suggest that the near-tip field should be a modification of that in Fig. 3, containing an additional plastic sector, of non-radial characteristics, adjoining the rear of the centered fan plastic sector. However, if the asymptotic analysis approach reviewed in Section 3 is employed to derive the near-tip fields, one cannot assemble such a four-sector near-tip field without violating the nonnegative plastic work requirement; this was stated without proof both by Dean and Hutchinson (1980) and by Rice (1982).

Thus, the Dean and Hutchinson (1980) and Freund and Douglas (1982) full-field solutions show that, at least to within the resolution of their detailed numerical analyses, the Chitaley and McClintock (1971) solution does not characterize small-scale yielding growing crack fields, and yet the near-tip solution structure suggested by these numerical solutions cannot be reproduced by the asymptotic analysis approach reviewed in Section 3. This suggests strongly that this asymptotic approach is not sufficiently general.

Based on this evidence, we now present a new, more robust approach for deriving the crack tip fields. Broadly, this approach will involve derivation of an *exact* representation of the stress and velocity field solution *everywhere* in a propagating plastic region comprised of non-centered characteristics, in terms of some initially-undetermined functions; such exact solution representations will be derived in the other regions too. Then, by enforcing continuity conditions and (second-order) asymptotics applied to these *solutions*, when a region of non-centered characteristics follows a propagating centered fan, we will derive an explicit representation of the near-tip fields in such a region and show that it can indeed be part of a complete near-tip solution.

4.2. *Exact solution representation in plastic region trailing a centered fan*

As just reviewed, the Dean and Hutchinson (1980) and Freund and Douglas (1982) numerical solutions show the presence of a substantial region of active plastic deformation, whose stress characteristics do *not* emanate from the crack tip, adjoining the trailing boundary of a centered fan plastic sector near a growing Mode III crack. The anti-plane strain governing equations are sufficiently manageable to allow an *exact* representation of the stress and velocity field solution in this region, in terms of some initially undetermined functions, as will now be shown.

With reference to Fig. 6, suppose a centered fan plastic Region A extends from ahead of the crack to an angle θ_1, where it is bordered by a plastic Region B containing non-radial stress characteristics. As suggested by the Dean–Hutchinson and Freund–Douglas numerics, Region B will border an elastic unloading Region C at a boundary

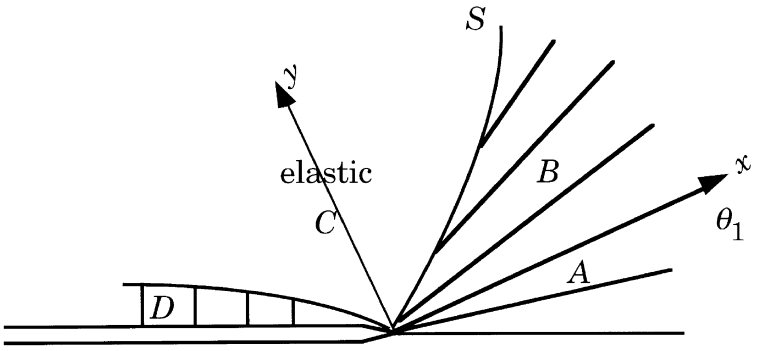

Fig. 6. Anticipated solution configuration, illustrating plastic Region B involving non-radial stress characteristics and introducing new Cartesian coordinate system x, y.

S, and we do anticipate a plastic reloading Region D due to the form (22) of the near-tip elastic sector stress fields. (The more accurate Freund–Douglas solution did capture such a small plastic reloading zone.) It will be convenient to introduce the new Cartesian coordinate system illustrated in Fig. 6, which is centered at the crack tip, moves with the growing crack and is oriented such that x lies along the rear fan boundary θ_1.

The exact solution for the fields in Region B is possible because, as was reviewed in Section 2, the stress characteristics must be straight lines everywhere in plastic regions. This means that in terms of the x, y Cartesian system of Fig. 6, the stress characteristics in Region B can be represented as:

$$y = \xi + m(\xi)x, \tag{32}$$

where ξ is the characteristic coordinate, i.e., it is (a different) constant along each characteristic. Equation (32) is obviously the equation of a family of straight lines, each of which has a y-intercept ξ and a slope m which in general is different for each characteristic. The function $m(\xi)$ is initially undetermined. We require stress continuity across $\theta = \theta_1$, which is $y = 0$; this line is a stress characteristic. This fact applied to (32) yields:

$$\text{On } y = 0, \quad m = \xi = 0 \quad \Rightarrow \quad m(0) = 0. \tag{33}$$

An exact stress field representation in Region B, in a form convenient for exact velocity field analysis, is now deduced by adapting the results (7)–(9): namely, if at an arbitrary point in Region B, ψ is defined to be the angle which the stress characteristic passing through that point makes with the x-axis, then the stress components in terms of the x, y system are:

$$\sigma_{x3} = -k \sin\psi, \quad \sigma_{y3} = k \cos\psi, \tag{34}$$

where by definition and application of (32)

$$\psi \equiv \arctan \frac{\mathrm{d}y}{\mathrm{d}x} = \arctan m(\xi). \tag{35}$$

Thus, substitution of (35) into (34) gives an exact stress field representation everywhere in Region B, with the only unknown being the function $m(\xi)$:

$$\boxed{\sigma_{x3} = -\frac{km(\xi)}{\sqrt{1+m^2(\xi)}}, \quad \sigma_{y3} = \frac{k}{\sqrt{1+m^2(\xi)}}}. \tag{36}$$

Observe that (36) satisfy stress continuity with the centered fan across $\theta = \theta_1$, since via (33) $\xi = 0$ and $m(0) = 0$ there.

To solve exactly for the velocity field everywhere in Region B, we apply the full form (5) of the flow rule, rewritten as

$$D_{i3} = \frac{1}{2G}(\dot{\boldsymbol{\tau}})_i + \dot{\Lambda}\tau_i, \tag{37}$$

where now i has range x, y, having defined

$$\boldsymbol{\tau} = \sigma_{x3}\mathbf{e}_x + \sigma_{y3}\mathbf{e}_y, \tag{38}$$

where $\mathbf{e}_x$, $\mathbf{e}_y$ are unit vectors in the x, y directions, respectively. In terms of the x, y coordinates, the steady-state simplification (6) applied to $\boldsymbol{\tau}$ becomes, using (38)

$$\begin{aligned}\dot{\boldsymbol{\tau}} &= -\dot{a}\frac{\partial \boldsymbol{\tau}}{\partial x_1} = -\dot{a}\left[\cos\theta_1 \frac{\partial \boldsymbol{\tau}}{\partial x} - \sin\theta_1 \frac{\partial \boldsymbol{\tau}}{\partial y}\right] \\ &= -\dot{a}\left(\cos\theta_1 \frac{\partial \sigma_{x3}}{\partial x} - \sin\theta_1 \frac{\partial \sigma_{x3}}{\partial y}\right)\mathbf{e}_x - \dot{a}\left(\cos\theta_1 \frac{\partial \sigma_{y3}}{\partial x} - \sin\theta_1 \frac{\partial \sigma_{y3}}{\partial y}\right)\mathbf{e}_y. \end{aligned} \tag{39}$$

By taking partial derivatives of (32) with respect to x and y, one calculates, respectively,

$$\frac{\partial \xi}{\partial x} = \frac{-m(\xi)}{1+xm'(\xi)}, \quad \frac{\partial \xi}{\xi y} = \frac{1}{1+xm'(\xi)}, \tag{40}$$

where a prime indicates differentiation with respect to a function's argument. Now, combining the two flow rule equations (37) to eliminate $\dot{\Lambda}$ gives

$$\sigma_{y3}\frac{\partial v_3}{\partial x} - \sigma_{x3}\frac{\partial v_3}{\partial y} = \frac{1}{G}(\sigma_{y3}\dot{\boldsymbol{\tau}}\cdot\mathbf{e}_x - \sigma_{x3}\dot{\boldsymbol{\tau}}\cdot\mathbf{e}_y). \tag{41}$$

This equation becomes, in terms of the exact stress field representation (36), using (39), (40) and simplifying

$$\frac{\partial v_3}{\partial x} + m\frac{\partial v_3}{\partial y} = -\dot{a}\frac{k}{G}\frac{m'(\xi)(\sin\theta_1 + m\cos\theta_1)}{[1+xm'(\xi)]\sqrt{1+m^2}}. \tag{42}$$

This is a linear first-order partial differential equation for v_3. To solve it, observe that the left side is the directional derivative along a stress characteristic:

$$\frac{\partial v_3}{\partial x} + m\frac{\partial v_3}{\partial y} = \sqrt{1+m^2}\,\mathbf{n}\cdot\nabla v_3 = \sqrt{1+m^2}\frac{\partial v_3}{\partial \eta}, \tag{43}$$

where we have defined $\mathbf{n}$ to be a unit vector directed along any characteristic:

$$\mathbf{n} = \frac{\mathbf{e}_x + m(\xi)\mathbf{e}_y}{\sqrt{1+m^2}}, \tag{44}$$

and η measures distance *along* any characteristic, so that on any specific characteristic in Region B,

$$\frac{x}{\eta} = \cos\psi = \cos(\arctan m) = \frac{1}{\sqrt{1+m^2}}. \tag{45}$$

Thus, (42) becomes, using (43) to rewrite its left side and (45) to substitute for x:

$$\frac{\partial v_3}{\partial \eta} = -\dot{a}\frac{k}{G}\frac{m'(\xi)(\sin\theta_1 + m\cos\theta_1)}{(1+m^2)\left[1+\dfrac{\eta m'(\xi)}{\sqrt{1+m^2}}\right]}. \tag{46}$$

This can now be integrated along any characteristic, where ξ is constant; doing so, and then using (45) to express η in terms of x gives the solution

$$\boxed{v_3 = \dot{a}\frac{k}{G}\left\{-\frac{(\sin\theta_1 + m\cos\theta_1)}{\sqrt{1+m^2}}\ln\left[xm'(\xi)+1\right] + F(\xi)\right\}}, \tag{47}$$

where $F(\xi)$ is an undetermined function of integration. It is straightforward to verify, by substitution and use of (40), that (47) is indeed the general solution to (42); that is, it is an exact representation of the velocity field everywhere in Region B of Fig. 6.

To derive an exact expression for $\dot{\Lambda}$ in Region B, return to the full form (37) of the flow rule; writing the $i = y$ component and solving for $\dot{\Lambda}$ gives:

$$\dot{\Lambda} = \frac{1}{2\sigma_{y3}}\left[\frac{\partial v_3}{\partial y} - \frac{1}{G}\dot{\mathbf{t}}\cdot\mathbf{e}_y\right]. \tag{48}$$

Using (36), (39), (40), (47) and simplifying, (48) becomes

$$\boxed{\begin{aligned}\dot{\Lambda} = \frac{\dot{a}}{2G[xm'(\xi)+1]}\Bigg\{&\frac{m'(\xi)(m\sin\theta_1 - \cos\theta_1)}{1+m^2}\ln\left[xm'(\xi)+1\right] \\ &+ (\sin\theta_1 + m\cos\theta_1)\left[\frac{mm'(\xi)}{1+m^2} - \frac{xm''(\xi)}{xm'(\xi)+1}\right] + \sqrt{1+m^2}F'(\xi)\Bigg\}.\end{aligned}} \tag{49}$$

4.3. *Enforcement of continuity conditions with centered fan sector*

We have shown that the exact stress, velocity and $\dot{\Lambda}$ field solutions everywhere in Region B of Fig. 6 are (36), (47) and (49). These solutions involve two as-yet undetermined functions, $m(\xi)$ and $F(\xi)$. We now show that enforcement of appropriate continuity conditions with the centered fan sector will enable determination of substantial information about these functions.

Stress continuity with Region A of Fig. 6 (i.e., across $\theta = \theta_1$) has already been enforced; this led to condition (33). The elastic–plastic discontinuity analysis of

Drugan and Rice (1984), which was rigorously substantiated and extended by Drugan (1998), proves that *all* stress components must be continuous across a propagating boundary such as $\theta = \theta_1$ here. Their analysis does not rule out a v_3 jump across this boundary provided it produces positive plastic work, but the Dean–Hutchinson (1980) and Freund–Douglas (1982) numerical solutions show no evidence of such a jump, so solutions with continuous v_3 will be sought here. Thus, noting that (33) reminds that to approach $\theta = \theta_1$ from within Region B one takes the limit as $\xi \to 0$, we next require that the exact velocity field expressions (26) and (47) be equal along $\theta = \theta_1$; this gives the condition

$$\lim_{\xi\to 0}\left\{-\frac{(\sin\theta_1 + m\cos\theta_1)}{\sqrt{1+m^2}}\ln\left[xm'(\xi)+1\right]+F(\xi)\right\} = \sin\theta_1\ln\left(\frac{R}{x}\right)+f(\theta_1) \tag{50}$$

for all x from the crack tip to the elastic–plastic boundary. One must contemplate the three possibilities for $m'(\xi)$ as $\xi \to 0$: $m'(\xi) \to 0$; $m'(\xi) \to$ constant; $m'(\xi) \to \infty$. A little analysis shows that only the last of these will permit (50) to be satisfied, and this will in addition require a specific asymptotic form for $F(\xi)$. Thus, velocity continuity (50) requires

$$m'(\xi) \to \infty \quad \text{as } \xi \to 0 \tag{51a}$$

and

$$F(\xi) \to \frac{(\sin\theta_1 + m\cos\theta_1)}{\sqrt{1+m^2}}\ln\left[Rm'(\xi)\right]+f(\theta_1+\operatorname{arcsinh}(m)) \quad \text{as } \xi \to 0, \tag{51b}$$

where we have retained terms in $F(\xi)$ that vanish as $\xi \to 0$ which will nevertheless permit $\dot{\Lambda}$ continuity across θ_1.

For $\xi \to 0$, (33) and (51) render (47) and (49) more explicit:

$$v_3 = \dot{a}\frac{k}{G}\left\{\frac{\sin\theta_1 + m\cos\theta_1}{\sqrt{1+m^2}}\ln\left[\frac{Rm'(\xi)}{xm'(\xi)+1}\right]+f(\theta_1)\right\} \quad \text{as } \xi \to 0, \tag{52}$$

$$\dot{\Lambda} = \frac{\dot{a}m'(\xi)}{2G[xm'(\xi)+1]}\left\{\frac{1}{1+m^2}(\cos\theta_1 - m\sin\theta_1)\ln\left[\frac{Rm'(\xi)}{xm'(\xi)+1}\right]\right.$$
$$\left.+(\sin\theta_1+m\cos\theta_1)\left[\frac{m}{1+m^2}+\frac{m''(\xi)}{m'^2(\xi)[xm'(\xi)+1]}\right]+f'(\theta_1)\right\} \quad \text{as } \xi \to 0. \tag{53}$$

Thus, making use of (33) and (51a), observe that for $\xi \to 0$ for any fixed x, (52) does indeed reduce to (26) evaluated on $\theta = \theta_1$, while taking the same limit of (53) results in

$$\dot{\Lambda} = \frac{\dot{a}}{2Gx}\left\{\cos\theta_1\ln\left(\frac{R}{x}\right)+(\sin\theta_1+m\cos\theta_1)\frac{m''(\xi)}{xm'^3(\xi)}+f'(\theta_1)\right\} \quad \text{as } \xi \to 0 \quad \text{for fixed } x, \tag{54}$$

which reduces to (27) evaluated on $\theta = \theta_1$, provided that

$$\lim_{\xi \to 0} \left\{ \frac{m''(\xi)}{m'^3(\xi)} \right\} = 0. \tag{55}$$

4.4. *Can Region B have finite angular extent for* $r \to 0$*?*

Let us assume first that Region B of Fig. 6 subtends a finite angular extent for $r \to 0$, terminating at $\theta = \theta_2$, say (where this is *not* the same θ_2 of the Chitaley–McClintock solution summarized earlier). On any ray within Region B, say $\theta = \theta^*$, where $\theta_1 < \theta^* < \theta_2$, we have

$$y = x \tan(\theta^* - \theta_1). \tag{56}$$

Combining this with (32), the equation of Region B's characteristics, and expressing the result in terms of the polar coordinate system of Fig. 1 gives:

$$\xi = y - m(\xi)x = y[1 - m(\xi)\cot(\theta^* - \theta_1)] = r\sin(\theta^* - \theta_1)[1 - m(\xi)\cot(\theta^* - \theta_1)]. \tag{57}$$

As $r \to 0$ along any ray $\theta = \theta^*$ in Region B, $\xi \to 0$ (consider Fig. 6), so that $m(\xi) \to 0$ via (33); thus along any such ray, (57) shows that asymptotically:

$$\xi = r\sin(\theta^* - \theta_1) \quad \text{as } r \to 0 \text{ along } \theta = \theta^*. \tag{58}$$

In order that Region B can have a finite angular extent for $r \to 0$, it must satisfy the condition that $\dot{\Lambda} \geqslant 0$. Let us examine (53) for $r \to 0$ along any ray $\theta = \theta^*$ in Region B. To facilitate this, observe via (58) that

$$xm'(\xi) = \cos(\theta^* - \theta_1) rm'(r\sin(\theta^* - \theta_1)) \to 0 \quad \text{as } r \to 0 \text{ along } \theta = \theta^* \tag{59}$$

due to (33). Thus, applying (33), (51a) and (59), the leading-order terms in (53) as $r \to 0$ along any ray $\theta = \theta^*$ in Region B are:

$$\dot{\Lambda} = \frac{\dot{a}}{2G} \left\{ \cos\theta_1 m'(\xi) \ln[Rm'(\xi)] + \sin\theta_1 \frac{m''(\xi)}{m'(\xi)} \right\} \quad \text{as } r \to 0 \text{ along } \theta = \theta^*. \tag{60}$$

Thus, for $\dot{\Lambda} \geqslant 0$ we must have, recalling that $\xi \to 0$ as $r \to 0$ along $\theta = \theta^*$:

$$m''(\xi) + \cot\theta_1 m'^2(\xi) \ln[Rm'(\xi)] \geqslant 0 \quad \text{as } \xi \to 0. \tag{61}$$

It is proved in the Appendix that no $m(\xi)$ exists that satisfies (61) together with (33) and (51a); thus, Region B *cannot* subtend finite angular extent in the $r \to 0$ limit.

4.5. *Determination of Region B's unloading boundary*

We have just proved that Region B cannot subtend finite angular extent all the way to the crack tip, yet the Dean–Hutchinson and Freund–Douglas numerical results reviewed above show that Region B has significant angular extent (about 30°, according to the more accurate Freund–Douglas results) down to a very small distance from the crack tip. The only possibility permitting reconciliation of these two facts is that the boundary (labeled S in Fig. 6) between Region B and the elastic Region C following it must coincide with the fan boundary $\theta = \theta_1$ at $r = 0$, but curve strongly

away from it, toward increasing θ, for $r > 0$. We now show that this is indeed the case, and derive an explicit asymptotic representation for this boundary S.

A specific representation for the function $m(\xi)$ in Region B cannot be derived from a near-tip analysis alone: this function depends on the far-field loading and geometry of the specimen, and is determined by continuity conditions across the elastic–plastic boundary between Region B and the outer elastic field (see Fig. 4; the more accurate Freund–Douglas numerical solution, Fig. 5, does not exhibit the concavity of the trailing elastic–plastic boundary in this figure). Thus, $m(\xi)$ can only be derived from a full-field solution of the growing crack problem, which is not feasible analytically. Nevertheless, enforcement of stress and velocity continuity with the centered fan sector provided two strong conditions, (33) and (51a), on the asymptotic structure of $m(\xi)$:

$$m(\xi) \to 0 \quad \text{and} \quad m'(\xi) \to \infty \quad \text{as } \xi \to 0. \tag{62}$$

Perhaps the simplest form for $m(\xi)$ that satisfies these conditions while retaining a fair degree of generality is

$$m(\xi) = \left(\frac{\xi}{b}\right)^p, \quad 0 < p < 1, \quad b > 0. \tag{63}$$

Here, the parameters b and p are as yet unspecified; it will turn out that b, which has length dimensions, can only be determined by matching with far-field conditions, and hence represents how the near-tip fields are affected by far-field loading and specimen geometry.

An additional restriction on form (63) is imposed by the requirement $\dot{\Lambda} \geqslant 0$ for $\xi \to 0$ at any fixed x; (54) shows this is guaranteed only if p is restricted to the range

$$0 < p < \tfrac{1}{2}. \tag{64}$$

With p in this range, (63) satisfies (55), so that $\dot{\Lambda}$ is continuous across θ_1 [it is >0 there, as shown by (54) with (55)].

The shape of boundary S, which divides Region B from the elastic unloading Region C, can now be determined. One relation valid along S is the equation of Region B's characteristics which, substituting (63) into (32), is

$$y = \xi + \left(\frac{\xi}{b}\right)^p x \quad \text{along } S. \tag{65}$$

The other condition we impose is that $\dot{\Lambda} = 0$ along S: although strictly speaking this is not required in nonhardening material, it will be true in the presence of even the slightest hardening, so that a nonhardening solution with this feature can be regarded as the expected limiting result of a hardening solution as hardening vanishes. Indeed, this is precisely the way the numerical procedures of Dean–Hutchinson and Freund–Douglas obtain the nonhardening solution, so it would appear that our attempt to analytically rationalize these numerical solutions should enforce this condition. Substitution of (63) into (53) and requiring $\dot{\Lambda} = 0$ gives an equation for ξ along S. [Use of (53) is valid because we have shown that S must approach θ_1 as $r \to 0$, hence

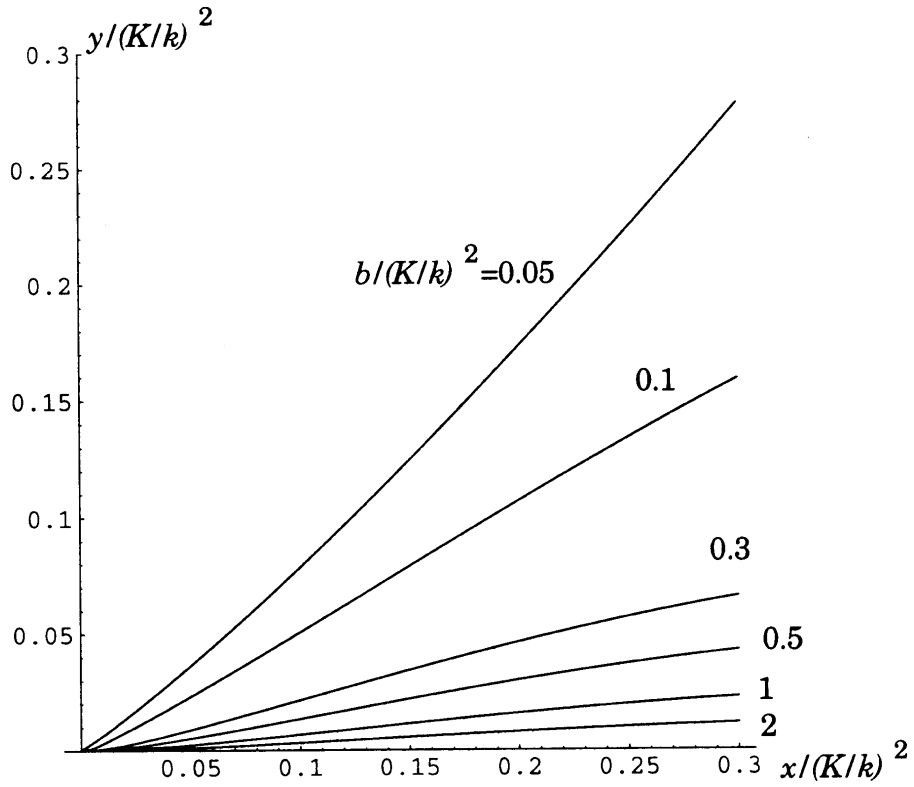

Fig. 7. Location and shape of boundary S of Fig. 6 with respect to the x, y coordinates of that figure, for a range of admissible values of the parameter b.

$\xi \to 0$ as $r \to 0$ along S.] The complete form of this equation is not solvable analytically. Thus, we shall pursue two approaches: we will solve this full equation numerically for ξ; and we will solve an asymptotic ($r \to 0$ along S) version of it analytically. In both approaches, the results for ξ as a function of x are substituted into (65), which is then an equation for the shape of S.

Figure 7 displays the results of the accurate numerical determination of boundary S just described, with $p = 0.346425$ for reasons derived later and using the small-scale yielding value in (30) for R to facilitate comparison with the finite element solutions; the abscissa and ordinate of Fig. 7 are the x, y axes of Fig. 6. Boundary S is plotted for several b values within its admissible range $0 < b < \infty$. Observe that for $\bar{b} \equiv b/(K/k)^2$ values above about 1, the boundary is essentially indistinguishable from the Sector A/B boundary ($\theta = \theta_1$ in Fig. 6, which is the abscissa here) for a significant distance from the crack tip. However, somewhat below $\bar{b} \approx 1$, the tangency of the two boundaries becomes indistinguishable on the scale shown (which corresponds to the plastic zone size; see Fig. 5), and the boundary shape becomes almost a straight line that makes an increasingly larger angle with the abscissa as $\bar{b}$ continues to increase. Thus, for $\bar{b}$-values lower than about 0.5, say, Region B has a significant angular extent

to within an extremely small radius from the crack tip, and hence the Chitaley–McClintock solution has questionable physical validity, whenever R differs little from (30).

To determine an analytical expression for boundary S, we perform an asymptotic analysis for $r \to 0$ along S. First, note from the analysis in Section 4.4 that it is not possible to find S having $\dot{\Lambda} = 0$ if $xm'(\xi) \to 0$ (or a constant, by a slight generalization) as $r \to 0$ along S. Thus, S must be shaped such that

$$xm'(\xi) \to \infty \quad \text{as } r \to 0 \text{ along } S. \tag{66}$$

When (66) is satisfied, the leading-order terms in $\dot{\Lambda}$ from (53) are:

$$\dot{\Lambda} = \frac{\dot{a}}{2Gx}\left\{\cos\theta_1 \ln\frac{R}{x} + \sin\theta_1 \frac{m''}{xm'^3} + f'(\theta_1)\right\} \quad \text{as } r \to 0 \text{ along } S, \tag{67}$$

so that $\dot{\Lambda} = 0$ gives the requirement:

$$\frac{1}{x^2}\frac{m''}{m'^3} + \cot\theta_1 \frac{1}{x}\ln\frac{\rho}{x} = 0 \quad \text{as } r \to 0 \text{ along } S, \tag{68}$$

where

$$\rho \equiv R\exp\left[\frac{f'(\theta_1)}{\cos\theta_1}\right]. \tag{69}$$

Substituting $m(\xi)$ from (63) into (68) and then solving for ξ gives (retaining only the dominant term):

$$\frac{\xi}{b} \sim \left[\frac{p^2}{1-p}\cot\theta_1 \frac{x}{b}\ln\frac{\rho}{x}\right]^{1/(1-2p)} \quad \text{as } r \to 0 \text{ along } S. \tag{70}$$

Using (70) and (63), one confirms that (66) is indeed satisfied for any p in the range (64). Thus, substituting for ξ from (70), (65) gives the near-tip equation for boundary S:

$$\frac{y}{b} = \left[\frac{p^2}{1-p}\cot\theta_1\right]^s \left(\frac{x}{b}\right)^{s+1}\left(\ln\frac{\rho}{x}\right)^s \quad \text{as } r \to 0 \text{ along } S, \tag{71}$$

where we have defined

$$s = \frac{p}{1-2p}. \tag{72}$$

Observe that (71) asymptotes to $y = 0$, i.e., to $\theta = \theta_1$, as required. It will also prove convenient to represent S in polar form, as:

$$\theta = \theta_1 + q_1(r) \quad \text{as } r \to 0 \text{ along } S. \tag{73}$$

Then

$$y = r\sin(\theta-\theta_1) \sim rq_1(r), \quad x = r\cos(\theta-\theta_1) \sim r \quad \text{as } r \to 0 \text{ along } S, \tag{74}$$

so that (71) shows

$$q_1(r) = \left[\frac{p^2}{1-p}\cot\theta_1 \frac{r}{b}\ln\frac{\rho}{r}\right]^s \quad \text{as } r \to 0 \text{ along } S. \tag{75}$$

For the specific case of small-scale yielding crack growth, R and $f(\theta)$ are given by (30), so that from (69)

$$\rho = R\exp\left[\ln(\cos\theta_1) - \tan^2\theta_1\right] = 0.664\left(\frac{K}{k}\right)^2. \tag{76}$$

Result (70), with (63) and (74), show upon substitution into (36) and (52) that through second-order as $r \to 0$ along S, the stresses and velocity are:

$$\sigma_{x3} = -k\left[\frac{p^2}{1-p}\cot\theta_1 \frac{r}{b}\ln\frac{\rho}{r}\right]^s,$$

$$\sigma_{y3} = k - \frac{k}{2}\left[\frac{p^2}{1-p}\cot\theta_1 \frac{r}{b}\ln\frac{\rho}{r}\right]^{2s}, \tag{77}$$

$$v_3 = \dot{a}\frac{k}{G}\left[\sin\theta_1 \ln\frac{R}{r} + f(\theta_1) + \frac{\cos\theta_1}{s+1}\left(\frac{p^2}{1-p}\cot\theta_1 \frac{r}{b}\right)^s \left(\ln\frac{\rho}{r}\right)^{s+1}\right]. \tag{78}$$

5. HIGHER-ORDER STRESS AND VELOCITY FIELDS

5.1. *Exact representation of growing crack fields*

As shown in Section 3.2, eqns (24), (26), (27) give the exact representation for the stress, velocity and $\dot{\Lambda}$ fields everywhere in the centered fan sector, Region A of Fig. 6, from the crack tip all the way to the elastic–plastic boundary.

In Region B of Fig. 6, we have shown that the stress, velocity and $\dot{\Lambda}$ fields have the exact representations (36), (47) and (49), in terms of the undetermined functions $m(\xi)$, $F(\xi)$. When conditions (33) and (51) are used, v_3 and $\dot{\Lambda}$ specify to (52), (53). Form (63) enables complete determination of the stress, velocity and $\dot{\Lambda}$ fields in Region B, at least for $\xi \to 0$: substitution of (63) into (32) gives the characteristics' equations everywhere in this region as

$$y = \xi + \left(\frac{\xi}{b}\right)^p x. \tag{79}$$

With b determined for a specific far-field geometry and loading, (79) is solved for $\xi = \xi(x, y)$, and this result is substituted into (63). The stress fields are then given by (36), while v_3 and $\dot{\Lambda}$ are given by (52), (53). Note that the solution of (79) for $\xi = \xi(x, y)$, and hence the representation of the stress, velocity and $\dot{\Lambda}$ fields, is impossible in closed form.

An exact representation of the stress and velocity fields in Region C of Fig. 6, the elastic unloading region, is also possible in terms of undetermined functions. The complete governing equations are, from (2a), (4a), (5) with $\dot{\Lambda} = 0$, and (6):

$$\frac{\partial \sigma_{13}}{\partial x_1} + \frac{\partial \sigma_{23}}{\partial x_2} = 0, \quad \frac{\partial v_3}{\partial x_1} = -\frac{\dot{a}}{G}\frac{\partial \sigma_{13}}{\partial x_1}, \quad \frac{\partial v_3}{\partial x_2} = -\frac{\dot{a}}{G}\frac{\partial \sigma_{23}}{\partial x_1}. \tag{80a,b,c}$$

These are solved exactly, as follows: equating $\partial^2 v_3/\partial x_1 \partial x_2$ as calculated from each of (80b,c) and using (80a) to eliminate σ_{13} gives

$$\left(\frac{\partial^2}{\partial x_1^2} + \frac{\partial^2}{\partial x_2^2}\right)\sigma_{23} = 0, \tag{81}$$

the general solution to which can be represented as the real part of an arbitrary analytic function $w(z)$, where $z = x_1 + \mathrm{i}x_2$, with i being the imaginary unit:

$$\sigma_{23} = k\,\mathrm{Re}\,[w(z)]. \tag{82}$$

Then using this in (80a) gives

$$\frac{\partial \sigma_{13}}{\partial x_1} = -\frac{\partial \sigma_{23}}{\partial x_2} = -k\,\mathrm{Re}\,[w'(z)\mathrm{i}] = k\,\mathrm{Im}\,[w'(z)] \quad \Rightarrow \quad \sigma_{13} = k\{\mathrm{Im}\,[w(z)] + g(x_2)\}, \tag{83}$$

where $g(x_2)$ is an arbitrary function. Thus, combining (82) and (83), we have

$$\boxed{\sigma_{23} + \mathrm{i}\sigma_{13} = k\{w(z) + \mathrm{i}g(x_2)\}}. \tag{84}$$

To solve for v_3, integrate (80b) with respect to x_1, use (83) for σ_{13}, and substitute the resulting expression for v_3 into (80c), using (82) for σ_{23}. The result is:

$$\boxed{v_3 = -\dot{a}\frac{k}{G}\,\mathrm{Im}\,[w(z)]}. \tag{85}$$

Thus, (84), (85) are exact representations for the stress and velocity fields everywhere in Region C in terms of the undetermined functions $w(z)$ and $g(x_2)$.

For Region D of Fig. 6, the plastic reloading region, the traction-free crack face condition requires that $\sigma_{23} = 0$ on $x_2 = 0$, $x_1 < 0$. The facts that this region is at yield and that the stress characteristics must be straight lines (Section 2) show that the exact stress field everywhere in this region must be (choosing the sign to agree with the Chitaley–McClintock solution)

$$\boxed{\sigma_{13} = k, \quad \sigma_{23} = 0}. \tag{86}$$

The flow rule (5) is, using (4a) and (6):

$$\frac{\partial v_3}{\partial x_\alpha} = -\frac{\dot{a}}{G}\frac{\partial \sigma_{\alpha 3}}{\partial x_1} + 2\dot{\Lambda}\sigma_{\alpha 3}, \quad \alpha = 1, 2, \tag{87}$$

where the first right-side term is identically zero via (86). Thus, solving (87) first for $\alpha = 2$ and then for $\alpha = 1$, using (86), gives the results:

$$\boxed{v_3 = \dot{a}\frac{k}{G}h(x_1)}, \tag{88}$$

$$\boxed{\dot{\Lambda} = \frac{\dot{a}}{2G}h'(x_1)}, \tag{89}$$

where $h'(x_1) \geqslant 0$ to satisfy $\dot{\Lambda} \geqslant 0$ but is otherwise undetermined. (Note that for the other sign choice in (86), $\dot{\Lambda} \geqslant 0$ would require $h'(x_1) \leqslant 0$ from (89), which via (88) is physically implausible.) Thus, (86), (88), (89) are exact representations of these fields everywhere in Region D, in terms of the undetermined function $h(x_1)$.

5.2. *Higher-order asymptotic analytical representation of fields in Regions C, D*

As noted earlier, it does not seem possible to specify analytically in closed form the undetermined functions in the above exact representations for the fields *everywhere* in Regions B–D.

As an alternative, the forms (77), (78) suggest that an explicit analytical representation for these fields in Regions C and D can be determined asymptotically, for $r \to 0$. (Apparently for Region B, one must work with the full representation derived earlier for this region.) Beginning with Region C, it appears simplest to rewrite the functions appearing in the general solution representations (84), (85) as:

$$w(z) = \mathrm{i}B\ln\frac{R}{z} + A + w^*(z), \tag{90}$$

$$g(x_2) = -B\ln\frac{R}{x_2} + C + g^*(x_2), \tag{91}$$

where the starred functions vanish as $r \to 0$. The terms containing the (real) constants A, B, C correspond to the leading-order solution given earlier in (22).

The fields in Region C are thus:

$$\begin{aligned}\sigma_{23} &= k[A + B\theta + \mathrm{Re}\, w^*(z)],\\ \sigma_{13} &= k[C + B\ln|\sin\theta| + \mathrm{Im}\, w^*(z) + g^*(x_2)],\end{aligned} \tag{92}$$

$$v_3 = -\dot{a}\frac{k}{G}\left[B\ln\frac{R}{r} + \mathrm{Im}\, w^*(z)\right]. \tag{93}$$

The fields in Region D are given by (86) and (88), the latter of which we rewrite as

$$\boxed{v_3 = -\dot{a}\frac{k}{G}\left[B\ln\left(\frac{R}{x_1}\right) + h^*(x_1)\right]}, \tag{94}$$

where $h^*(x_1) \to 0$ as $r \to 0$. Furthermore, we represent the boundaries of Region C as:

$$S: \quad \theta = \theta_1 + q_1(r), \tag{95}$$

$$S_{\mathrm{CD}}: \quad \theta = \theta_2 + q_2(r), \tag{96}$$

where $q_1(r)$, $q_2(r) \to 0$ as $r \to 0$, and S_{CD} represents the boundary between Regions C and D.

Finally, using (77) and (78), the fields through second order for $r \to 0$ along S, derived from Region B, are:

$$\sigma_{13} = \sigma_{x3}\cos\theta_1 - \sigma_{y3}\sin\theta_1 = -k\sin\theta_1 - k\cos\theta_1\left[\frac{p^2}{1-p}\cot\theta_1\frac{r}{b}\ln\frac{\rho}{r}\right]^s,$$

$$\sigma_{23} = \sigma_{x3}\sin\theta_1 + \sigma_{y3}\cos\theta_1 = k\cos\theta_1 - k\sin\theta_1\left[\frac{p^2}{1-p}\cot\theta_1\frac{r}{b}\ln\frac{\rho}{r}\right]^s, \tag{97}$$

$$v_3 = \dot{a}\frac{k}{G}\left[\sin\theta_1\ln\frac{R}{r} + f(\theta_1) + \frac{\cos\theta_1}{s+1}\left(\frac{p^2}{1-p}\cot\theta_1\frac{r}{b}\right)^s\left(\ln\frac{\rho}{r}\right)^{s+1}\right]. \tag{98}$$

Now, stress and velocity continuity through second-order along S and S_{CD} give the values of leading-order results summarized in (31) and Fig. 3 [one of which is that $B = -\sin\theta_1$], and the following second-order conditions (i.e., neglecting higher-order terms), having employed (75) with (86) and (92)–(98):

$$\mathrm{Re}\, w^*(r\,\mathrm{e}^{\mathrm{i}\theta_1}) = 0, \tag{99a}$$

$$\mathrm{Im}\, w^*(r\,\mathrm{e}^{\mathrm{i}\theta_1}) = -g^*(r\sin\theta_1) = -\frac{\cos\theta_1}{s+1}\left(\frac{p^2}{1-p}\cot\theta_1\frac{r}{b}\right)^s\left(\ln\frac{\rho}{r}\right)^{s+1}, \tag{99b,c}$$

$$-\sin\theta_1 q_2(r) + \mathrm{Re}\, w^*(r\,\mathrm{e}^{\mathrm{i}\theta_2}) = 0, \tag{99d}$$

$$-\sin\theta_1\cot\theta_2 q_2(r) + \mathrm{Im}\, w^*(r\,\mathrm{e}^{\mathrm{i}\theta_2}) + g^*(r\sin\theta_2) = 0, \tag{99e}$$

$$\mathrm{Im}\, w^*(r\,\mathrm{e}^{\mathrm{i}\theta_2}) = h^*(r\cos\theta_2). \tag{99f}$$

These suggest that we attempt to satisfy (99) with second-order functions of the forms:

$$w^*(z) = (C_1 + \mathrm{i}C_2)\left(\frac{z}{b}\right)^s\left(\ln\frac{\rho}{z}\right)^{s+1}, \tag{100}$$

$$g^*(x_2) = C_3\left(\frac{x_2}{b}\right)^s\left(\ln\frac{\rho}{x_2}\right)^{s+1}. \tag{101}$$

We shall use the fact that, for $r \to 0$,

$$\left(\ln\frac{\rho}{z}\right)^{s+1} = \left(\ln\frac{\rho}{r}\right)^{s+1}\left(1 - \frac{\mathrm{i}\theta}{\ln\dfrac{\rho}{r}}\right)^{s+1} = \left(\ln\frac{\rho}{r}\right)^{s+1} - \mathrm{i}(s+1)\theta\left(\ln\frac{\rho}{r}\right)^s + \cdots. \tag{102}$$

Then, substitution of (100), (101) into (99a–e) shows that the latter are satisfied to the order expressed if:

$$C_1 = -\frac{1}{s+1}\sin s\theta_1 \cos\theta_1 \left(\frac{p^2}{1-p}\cot\theta_1\right)^s, \tag{103a}$$

$$C_2 = \cot s\theta_1 C_1, \tag{103b}$$

$$C_3 = -\frac{C_1}{\sin s\theta_1 \sin^s \theta_1}, \tag{103c}$$

$$q_2(r) = \frac{1}{\sin\theta_1}(C_1 \cos s\theta_2 - C_2 \sin s\theta_2)\left(\frac{r}{b}\right)^s \left(\ln\frac{\rho}{r}\right)^{s+1}, \tag{103d}$$

$$\cos s(\theta_2-\theta_1) + \cot\theta_2 \sin s(\theta_2-\theta_1) - \left(\frac{\sin\theta_2}{\sin\theta_1}\right)^s = 0. \tag{103e}$$

The last condition, which arises from (99e) via substitution from (103a–d), determines admissible values of s, given that the leading-order solution specifies:

$$\theta_1 = 0.34402576, \quad \theta_2 = 3.1351945. \tag{104}$$

Solutions of (103e) having $s > 0$, as mandated by (64) with (72), are:

$$s = 1.12787, 2.25339, 3.37893, 4.50448, \ldots, \tag{105}$$

which via (72) correspond to p values of, in corresponding order:

$$p = 0.346425, 0.409203, 0.435549, 0.450045, \ldots \quad . \tag{106}$$

From (105) and the previous results, e.g. (77), (78), we see that the strongest second-order correction corresponds to the smallest admissible s-value, i.e., the first in (105), whose corresponding p-value is the first in the list (106). This is the reason for the use of this p-value in Fig. 7. We have thus determined, via (103) and the first of (105), (106), the complete second-order correction to the fields in Region C, except for specification of the parameters b and ρ. The values of these parameters are anticipated to change for different far-field loadings and specimen geometries. However, for the small-scale yielding steady-state crack growth case analyzed by Dean–Hutchinson and Freund–Douglas, ρ is given by (76), and observe from Fig. 7 that to match the Freund–Douglas unloading boundary location of $\theta \approx 50^\circ$ (which would correspond to an angle of $\approx 30^\circ$ in Fig. 7 since this is plotted with respect to the x, y coordinates of Fig. 6), we have

$$b \approx 0.1(\mathrm{K}/\mathrm{k})^2. \tag{107}$$

Thus, the stress and velocity fields through second order in Region C are given by (92) and (93) with (100), (101), (103a–d), (104), the first of (105), (106), and (76), (107).

In Region D, the stress field is exactly given by (86). To determine the velocity and $\dot{\Lambda}$ fields through second order in this sector, we use (100) to solve (99f) for $h^*(x_1)$, and employ (103a,b):

$$h^*(x_1) = -\frac{1}{s+1}\cos\theta_1 \cos s(\theta_2-\theta_1)\left(\frac{p^2}{1-p}\frac{\cot\theta_1}{\cos\theta_2}\frac{x_1}{b}\right)^s\left(\ln\frac{\rho\cos\theta_2}{x_1}\right)^{s+1}. \quad (108)$$

Thus, the velocity and $\dot{\Lambda}$ fields through second order are given by (88) and (89) with (104), the first of (105) and (106), (108) and the fact that we earlier defined

$$h(x_1) = -B\ln\left(\frac{R}{x_1}\right) - h^*(x_1). \quad (109)$$

ACKNOWLEDGEMENTS

Support of this work by the Applied Mathematics Program of the National Science Foundation under Grant DMS-9404492 is gratefully acknowledged. I thank my colleague, Professor M. C. Shen, for helpful discussions concerning the proof in the Appendix.

REFERENCES

Chitaley, A. D. and McClintock, F. A. (1971) Local criteria for ductile fracture. *Journal of the Mechanics and Physics of Solids* **19,** 147–163.

Dean, R. H. and Hutchinson, J. W. (1980) Quasi-static steady crack growth in small scale yielding. *Fracture Mechanics*. ASTM-STP 700, pp. 383–405.

Drugan, W. J. (1985) On the asymptotic continuum analysis of quasi-static elastic–plastic crack growth and related problems. *Journal of Applied Mechanics* **52,** 601–605.

Drugan, W. J. (1998) Thermodynamic equivalence of steady-state shocks and smooth waves in general media ; applications to elastic–plastic shocks and dynamic fracture. *Journal of the Mechanics and Physics of Solids* **46,** 313–336.

Drugan, W. J. and Rice, J. R. (1984) Restrictions on quasi-statically moving surfaces of strong discontinuity in elastic–plastic solids. In *Mechanics of Material Behavior*, ed. G. J. Dvorak and R. T. Shield, pp.59–73. Elsevier Science, Amsterdam.

Freund, L. B. and Douglas, A. S. (1982) The influence of inertia on elastic–plastic antiplane-shear crack growth. *Journal of the Mechanics and Physics of Solids* **30,** 59–74.

Rice, J. R. (1968) Mathematical analysis in the mechanics of fracture. In *Fracture* : *An Advanced Treatise*, ed. H. Leibowitz, Vol. 2, pp. 191–311. Academic Press, New York.

Rice, J. R. (1982) Elastic–plastic crack growth. In *Mechanics of Solids*: *The R. Hill* 60*th Anniversary Volume*, ed. H. G. Hopkins and M. J. Sewell, pp. 539–562. Pergamon Press, Oxford.

APPENDIX

Here we prove that no $m(\xi)$ exists that simultaneously satisfies (33), (51a) and (61), which are, respectively :

$$m(\xi) \to 0 \quad \text{as } \xi \to 0, \quad (A1)$$

$$m'(\xi) \to \infty \quad \text{as } \xi \to 0, \quad (A2)$$

$$m''(\xi) + \cot\theta_1 m'^2(\xi)\ln[Rm'(\xi)] \geqslant 0 \quad \text{as } \xi \to 0. \quad (A3)$$

Since it is easy to find an $m(\xi)$ that satisfies (A1) and (A2) but violates (A3), it is sufficient to show that no $m(\xi)$ exists satisfying (A1)–(A3) with the equality in (A3). Defining

$$n'(\xi) = Rm'(\xi), \tag{A4}$$

and multiplying (A3) with the equality by R gives

$$n''(\xi) + cn'^2(\xi) \ln [n'(\xi)] = 0 \quad \text{as } \xi \to 0, \tag{A5}$$

where we have defined the positive constant $c = \cot \theta_1 / R$. Separating (A5) and integrating gives

$$\int \frac{\mathrm{d}(n')}{n'^2 \ln(n')} = -c\xi \quad \text{as } \xi \to 0. \tag{A6}$$

We desire a solution to this for $\xi \to 0$, where $n' \to \infty$. In this limit, an integration by parts of (A6) shows

$$n' \ln(n') = \frac{1}{c\xi} \quad \text{as } \xi \to 0. \tag{A7}$$

Now define

$$f(y) \equiv y \ln y = \frac{1}{x}, \quad \text{where } y = n', \quad x = c\xi. \tag{A8}$$

We assume $0 < x < \infty$ and $1 < y < \infty$, and observe that for x in this range, $y = f^{-1}(1/x)$ exists. We examine whether $f^{-1}(1/x)$ is integrable at $x = 0$.

Consider the integral

$$I = \int_{\varepsilon}^{c} f^{-1}\left(\frac{1}{x}\right) \mathrm{d}x, \tag{A9}$$

where $0 < \varepsilon < c < \infty$. Using (A8), change x in I to y:

$$I = \int_{1/\varepsilon}^{1/c} (-x^2) f^{-1}\left(\frac{1}{x}\right) \mathrm{d}\left(\frac{1}{x}\right) = \int_{1/\varepsilon}^{1/c} \left[-\frac{1}{f^2(y)}\right] y \, \mathrm{d}f(y)$$

$$= \int_{f^{-1}(1/\varepsilon)}^{f^{-1}(1/c)} \frac{y(1+\ln y)\,\mathrm{d}y}{y^2 \ln^2 y}. \tag{A10}$$

Now, as $\varepsilon \to 0$, $f^{-1}(1/\varepsilon) \to \infty$, so that I becomes:

$$I = \int_{f^{-1}(1/c)}^{\infty} \frac{(1+\ln y)\,\mathrm{d}y}{y \ln^2 y} = \left[-\frac{1}{\ln y} + \ln(\ln y)\right]_{f^{-1}(1/c)}^{\infty}, \tag{A11}$$

which clearly diverges. Thus, $f^{-1}(1/x)$ is not integrable at $x = 0$. This proves, tracing back through (A8) and (A4), that if the minimal condition (A3) with equality sign is enforced, along with (A2), the resulting $m(\xi)$ cannot satisfy (A1).